DOI: 10.1038/s41565-022-01086-4

Laser-induced nanobubbles safely ablate vitreous opacities *in vivo*

Félix Sauvage[1+], Van Phuc Nguyen[2,6+], Yanxiu Li[2], Aranit Harizaj[1], J. Sebag[4,5], Dimitri Roels[7], Viktor Van Havere[1], Karen Peynshaert[1], Ranhua Xiong[8], Juan C. Fraire[1], Marie-José Tassignon[9], Katrien Remaut[1], Yannis M. Paulus[2,3]*, Kevin Braeckmans[1]*, Stefaan C. De Smedt[1,8]*

[1]Laboratory of General Biochemistry and Physical Pharmacy, Faculty of Pharmaceutical Sciences, Ghent University, 9000 Ghent, Belgium.

[2] Department of Ophthalmology and Visual Sciences, University of Michigan, Ann Arbor, MI, United States

[3] Department of Biomedical Engineering, University of Michigan, Ann Arbor, MI, United States

[4]VMR Institute for Vitreous Macula Retina, Huntington Beach, California 92647, United States

[5]Doheny Eye Institute/UCLA, Los Angeles, California 90033, United States

[6]NTT-Hitech Institutes, Nguyen Tat Thanh University, Ho Chi Minh City, Vietnam

[7]Department of Ophthalmology, Ghent University Hospital, 9000, Ghent, Belgium

[8] Joint Laboratory of Advanced Biomedical Materials (NFU-UGent), International Innovation for Center for Forest Chemicals and Materials, College of Chemical Engineering, Nanjing Forestry University (NFU), Nanjing 210037, P. R. China

[9]Department of Ophthalmology, Antwerp University Hospital, University of Antwerp, 2020, Antwerp, Belgium

* Corresponding authors

E-mail : stefaan.desmedt@ugent.be; ypaulus@med.umich.edu; kevin.braeckmans@ugent.be

Tel: +32 9 264 80 76, Fax: +32 9 264 81 89

Corresponding address: Ottergemsesteenweg 460, 9000 Ghent, Belgium

[+] These authors contributed equally to this work.

Abstract

In myopia, diabetes and aging, fibrous vitreous liquefaction and degeneration is associated with the formation of opacities within the vitreous body that cast shadows on the retina, appearing as ‘floaters’ to the patient. Vitreous opacities degrade contrast sensitivity function and can cause significant impairment in vision-related quality-of-life. This study introduces ‘nanobubble ablation’ for safe destruction of vitreous opacities. Following intravitreal injection, hyaluronic acid coated gold nanoparticles and indocyanine green, which is widely used as a dye in vitreoretinal surgery, spontaneously accumulate on collagenous vitreous opacities in the eyes of rabbits. Applying nanosecond laser pulses generates vapor nanobubbles which mechanically destroy the opacities in rabbit eyes and in patients specimens. Nanobubble ablation might offer a safe and efficient treatment to millions of patients suffering from debilitating vitreous opacities and paves the way for a highly safe use of pulsed lasers in the posterior segment of the eye.

Keywords: *floaters, ICG, gold nanoparticles, pulsed lasers, vitreous, ophthalmology, vapor nanobubbles, stimuli responsive, collagen aggregates, vision degrading myodesopsia*

Introduction

Proteins play a crucial role in the function of cells and organisms. The accumulation of misfolded proteins leads to insoluble toxic aggregates, as exemplified by the aggregation of amyloidogenic peptides in neurodegenerative disorders[1]. Other proteins can form aggregates inducing different pathologies, such as aggregation of collagen in the vitreous body of the myopic and aging eye[2]. Vitreous (**Figure 1Ai**), which is a highly hydrated, transparent gel (> 98% water), is maintained by a diluted network of long, thin collagen (type II, V, IX and XI) fibrils[2]. As **Figure 1Aii** illustrates, type IX collagen has chondroitin sulfate chains which extend away from the fibril surfaces[3]. In young and healthy eyes, the chondroitin sulfate chains are bound to anionic hyaluronan (HA; **Figure 1Aii**) which is believed to space apart the collagen fibrils, thereby preventing their aggregation[3]. With aging and in myopia, there is a progressive dissociation of HA from collagen[2,4] (**Figure 1Aiii)** which results in liquefaction of the vitreous gel[2]. Collagen fibrils cross-link and aggregate, while the displaced (hydrophilic) HA forms liquid vitreous[4]. When collagen aggregates become large, patients start to experience 'floaters' known as *vision degrading myodesopsia* (**Figure 1Aiii**) which have a negative impact on vision and quality-of-life[2,5]. According to a survey, eye floaters have been reported in up to 76% of persons, with 33% reporting noticeable impairment in vision[6]. Patients report floaters as severely debilitating[7] and are willing to take a 11% risk of death and a 7% risk of blindness to get rid of floater-related symptoms[8]. All too often, patients with symptomatic vitreous opacities are left untreated and must cope with their symptoms, inducing depression, stress, and anxiety[9]. Lastly, the prevalence of vitreous floaters will increase due to population aging and the global pandemic of myopia[10].

Currently, two therapeutic options are available for the treatment of floaters. Pars plana vitrectomy[11], introduced in the 1970s[12], is relatively safe but invasive and carries risks[13,14]. Photo-ablation employs high energy laser pulses (2−8 mJ per pulse; up to 1000 shots per opacity) with a neodymium yttrium garnet (YAG) laser[15] that result in the disruption of vitreous opacities[16]. It is not clear whether this treatment ablates the opacities, as opposed to just fragmenting them into smaller pieces. Furthermore, for safety reasons, YAG laser cannot be applied to opacities close to the retina, as photo-mechanical damage of the retina may occur[17]. Further, only 38% of patients treated with YAG laser had moderate improvement in symptoms[18]. There are also risks due to high levels of laser energy[19]. We hypothesize that methods which enable destruction of vitreous opacities at a much lower energy could represent a major advance.

In previous work, we focused on the physics[20] and applications of vapor nanobubbles (VNBs) generated when photosensitizing agents are irradiated with pulsed lasers[21–25]. Upon illumination of gold nanoparticles (AuNPs) with a laser pulse at a suitable wavelength, an ultra-fast increase in temperature occurs at their surface. This heating leads to the evaporation of the surrounding water and the formation of VNBs which expand and collapse within tens to hundreds of nanoseconds [21]. Following the interesting observation by Sebag and others of the affinity of HA to vitreous collagen (**Figure 1Aii,iii**)[4,26,27], we reasoned that coating AuNPs with HA could be a promising strategy to bind AuNPs to vitreous opacities primarily composed of collagen (**Figure 1Aiii**). We confirmed *ex vivo* that AuNPs coated with hyaluronic acid (HA-AuNPs) indeed cluster on vitreous opacities obtained from patients who underwent vitrectomy. Illumination with a nanosecond laser generated VNBs that destroyed the vitreous opacities[28].

Here, we investigate whether VNBs safely destroy vitreous opacities *in vivo* with the combined use of pulsed lasers and selected photosensitizers in rabbit eyes. While AuNPs are considered biocompatible, they are not biodegradable, which might limit their use *in vivo*. In addition, it has been reported that AuNPs fragment into smaller sized particles upon pulsed laser irradiation[29], which may cause genotoxic effects through DNA intercalation causing damage to intraocular tissues[30]. Recently, we observed that VNBs can be formed from nanoparticles loaded with indocyanine green (ICG), which is FDA-approved for intravenous injection in (choroidal) angiography[31] and used off-label by ophthalmologists to stain the inner limiting membrane during chromodissection[32]. As ICG is known to bind to collagen, we hypothesized that ICG might accumulate on collagenous vitreous opacities and generate VNBs upon laser irradiation, resulting in mechanical destruction, similar to AuNPs (**Figure 1B**). Furthermore, compared to HA-AuNPs (10 nm), which absorb light around 530 nm, ICG absorbs in the near-infrared region which has lower light absorption by biomolecules.

In this work, we investigate the ability of HA-AuNPs and ICG to destroy vitreous opacities irradiated with nanosecond laser pulses *in vivo*. To model endogenous vitreous opacities we injected collagen aggregates (which we termed ‘exogenous collagen opacities’) into the eyes of rabbits and found that VNBs generated from ICG and HA-AuNPs allow safe destruction of vitreous opacities at lower laser fluence than employed with YAG laser. To our knowledge, since the introduction of YAG laser in ophthalmology in 1977[33], ‘nanobubble-mediated ablation of eye floaters’ is the first concept proposed for a safer and efficient treatment of eye

floaters.

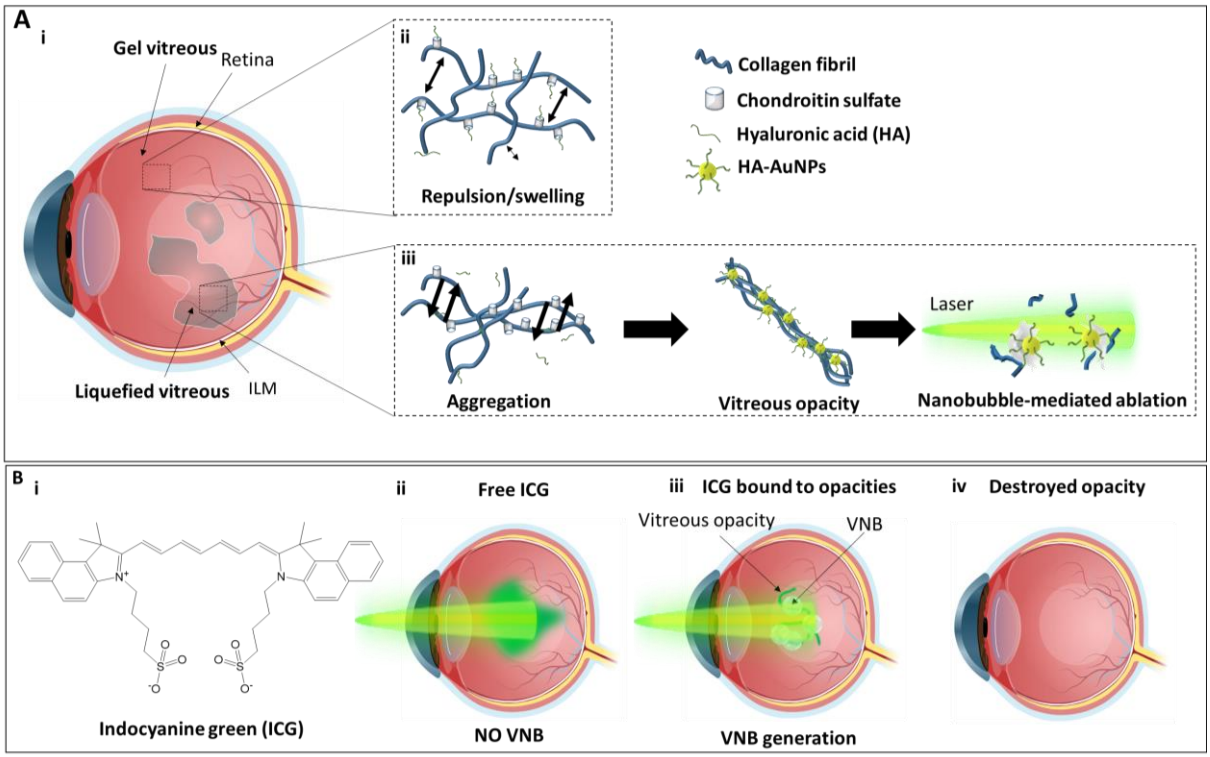

Figure 1. (A) Vitreous liquefaction (i) is due to a progressive dissociation of HA from the collagen fibrils (ii, iii) leading to the aggregation of the fibrils forming increasingly large vitreous opacities (iii)[2,4,26]. We previously showed *ex vivo* that coating AuNPs with HA targets vitreous opacities which are largely devoid of HA (iii). Upon irradiation with a pulsed laser, VNBs formed and then collapsed, mechanically destroying the opacities[28]. (B) We hypothesize that indocyanine green (ICG; (i)) that is known to bind to collagen will 'cluster' on vitreous opacities (ii, iii) and that subsequent laser irradiation of ICG will generate VNBs (preferentially) ablating the opacities. This should result in targeted 'nanobubble-mediated' ablation of the opacities (iv), leaving the surrounding vitreous untouched.

VNBs generated from HA-AuNPs ablate collagen opacities in vivo

In recent experiments, we observed that HA-AuNPs accumulate on vitreous opacities excised from patients during vitrectomy; pulsed laser irradiation of the opacities results in VNBs which mechanically destroy them (**Figure 2Ai-iii**)[28]. To investigate whether this approach allows destruction of vitreous opacities *in vivo*, we injected exogenous collagen opacities into the vitreous body of rabbit eyes (**Figure 2B**). The exogenous collagen opacities were injected close to the retina (<500 µm; as could be confirmed by OCT imaging, **Figure 2B**), to maximize the chances of detecting untoward effects. Five days after injection of the opacities, rabbits were

intravitreally injected with HA-AuNPs (**Figure 2Ci**); to allow their diffusion and binding to the exogenous collagen opacities in the vitreous body, we waited for another 3 days before treating the eyes with laser irradiation (**Figure 2Cii**).

Following intravitreal injection of HA-AuNPs, the exogenous collagen opacities became reddish (**Figure 2Ciii**; PAM, **Figure 2Civ**), due to accumulation of HA-AuNPs on the exogenous vitreous opacities. Opacities that were clearly visible by OCT before irradiation (**Figure 2Cv**), became less visible after 3 pulses (scans) and were no longer visible after 7 pulses. For all the rabbits (n=3) we observed that 5 +/- 2 pulses were sufficient to completely ablate the exogenous vitreous opacities. These results confirmed that light-induced VNBs generated upon laser irradiation of 10 nm HA-AuNPs can destroy collagen opacities in vitreous *in vivo*.

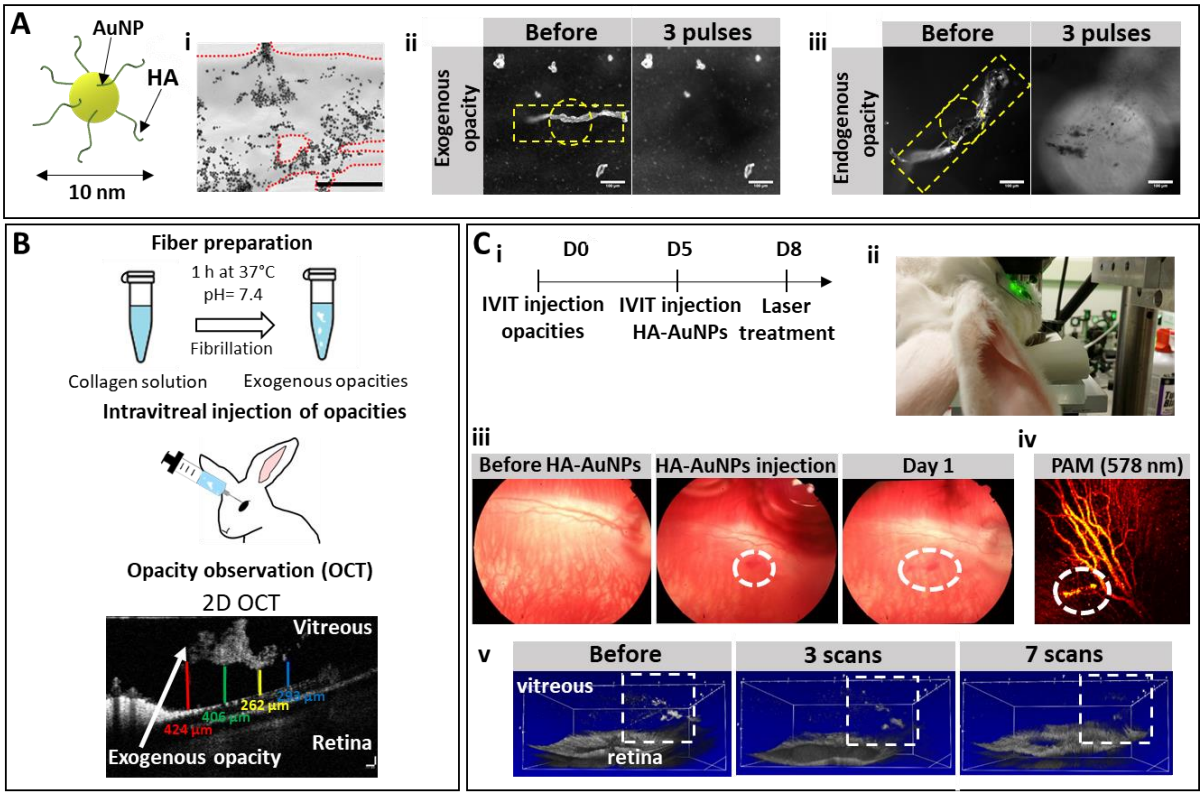

Figure 2. (A) HA-coated gold nanoparticles were found to accumulate on exogenous collagen opacities and human vitreous opacities obtained by vitrectomy in patients suffering from eye floaters. In (i) the red dotted lines represent the edges of an exogenous collagen opacity loaded with HA-coated gold nanoparticles (black dots). (ii, iii) Pulsed laser irradiation – *ex vivo* – of an exogenous collagen opacity (ii) and a human vitreous opacity (iii) ablates them (with permission from [28], Copyright 2019, ACS publications). The presented images are representative of 3 independent experiments. (B) The 'eye floater model' in rabbits: collagen

opacities were prepared *in vitro* (named exogenous collagen opacities) and injected intravitreally in anesthetized rabbits. OCT confirmed that exogenous collagen opacities were present close to the retina (distances to the retina are indicated). (C) (i) HA-AuNPs were injected intravitreally 5 days after intravitreal injection of the exogenous collagen opacities and eyes were treated with laser (532 nm; 1.9 J/cm²) 3 days later; (ii) Areas in the vitreous body of anesthetized rabbits (4.5×4.5 mm²) were scanned with the laser beam. (iii) Fundus observations revealed reddish collagen opacities (dotted white circle) suggesting accumulation of HA-AuNPs on the opacities, which was confirmed by PAM-imaging (iv; 578 nm). (v) OCT imaging revealed that pulsed laser irradiation destroyed the exogenous collagen opacities; after 7 laser pulses (scans) the collagen opacities were gone. For all the rabbits (n=3) we observed that 5 ± 2 (mean ± s.d.) pulses were sufficient to completely ablate the opacities.

VNBs generated from ICG ablate exogenous and human vitreous opacities

AuNPs are clinically studied for the treatment of various diseases[34] and are under investigation in ophthalmology for anti-inflammatory properties[35], enhanced imaging of ocular structures,[36] and drug delivery[37]. However, other photosensitizers able to generate VNBs are attractive for safe ablation of vitreous opacities, specifically the photosensitizing dye ICG, which is used in ophthalmology, seemed of interest[32]. We observed rather unexpectedly that VNBs can be formed when polymeric nanoparticles are loaded with ICG and irradiated with pulsed laser light (**Figure S1**). As ICG is known to bind to collagen, we hypothesized that ICG might spontaneously accumulate on collagenous opacities in the vitreous and generate VNBs upon laser irradiation. The color of exogenous collagen opacities changed upon mixing with ICG suggesting that ICG accumulated on the opacities **(Figure 3Ai)**. To determine whether laser irradiation of collagen-bound ICG could induce VNBs (**Figure 3Aii**), exogenous collagen opacities mixed with ICG were irradiated at a laser fluence of 4.5 J/cm² and observed by dark field microscopy (**Figure 3Aiii**). It clearly appeared that VNBs (observed as bright spots) formed. Subsequently, we measured the number of VNBs generated as a function of the fluence of the laser pulse (**Figure 3Aiv**) and found the VNB threshold (T90; see Methods) to be 3.3 J/cm². T10, which is the fluence of a single laser pulse at which 10% of the maximal number of VNBs is generated, equaled 1.2 J/cm². For fluences lower than T10, heat generation is predominant (heating mode); between T10 and T90 both heat and bubbles are generated (intermediate mode); for fluences higher than T90, VNB formation is the predominant phenomenon (bubble mode).

As illustrated in **Figure 3Bi**, 5 pulses at a fluence of 4.5 J/cm² were sufficient to destroy an exogenous collagen opacity while applying laser pulses without ICG had no effect. Besides, as shown in **Figure 3Bii**, it appears that at a higher fluence less pulses were required to fully destroy the opacities. In the heating mode (0.6 J/cm²), around 60 pulses were required to completely destroy an opacity; at a fluence of 2.2 J/cm² (intermediate mode) the number of pulses was around 9 while in the bubble mode (at a fluence of 4.5 J/cm²) on average 5 pulses were sufficient to destroy an opacity. Taken together, our results suggest that VNBs, and the mechanical forces associated with them, drastically lower the number of laser pulses needed to destroy collagen opacities. This supports the hypothesis that the mechanical forces induced by VNBs are the main reason for the breakdown of the opacities; i.e. a photomechanical effect seems far more efficient than a photothermal effect to destroy collagenous opacities. Of interest as well is that the average number of pulses to destroy an exogenous collagen opacity with ICG is similar to the average number needed when HA-AuNPs are used (at a same fluence of 4.5 J/cm²; **Figure 3Biii**). To support our observation that the collagen opacities become destroyed upon laser treatment, we performed turbidity experiments (**Figure S2**) on suspensions of collagen opacities. We therefore measured the UV-vis spectrum of (i) untreated opacities, (ii) opacities treated with ICG and irradiated with the pulsed laser and (iii) sonicated opacities (as a positive control). As shown in **Figure S2**, a clear decrease in absorbance was observed when opacities were treated with ICG and irradiated with the pulsed laser.

Next, we investigated whether ICG and laser pulses could destroy opacities present in vitreous samples that were obtained during vitrectomy in patients; note that such human vitreous opacities are collagenous, though they differ from the exogenous collagen opacities in composition, size and morphology. As illustrated in **Figure 3Ci**, human vitreous opacities were mixed with ICG (0.5 mg/mL in water) and were destroyed upon irradiation with one or two pulses at a fluence of 4.5 J/cm² (**Figure 3Cii)**, consistent with previous observations using HA-AuNPs (**Figure 2A**)[28].

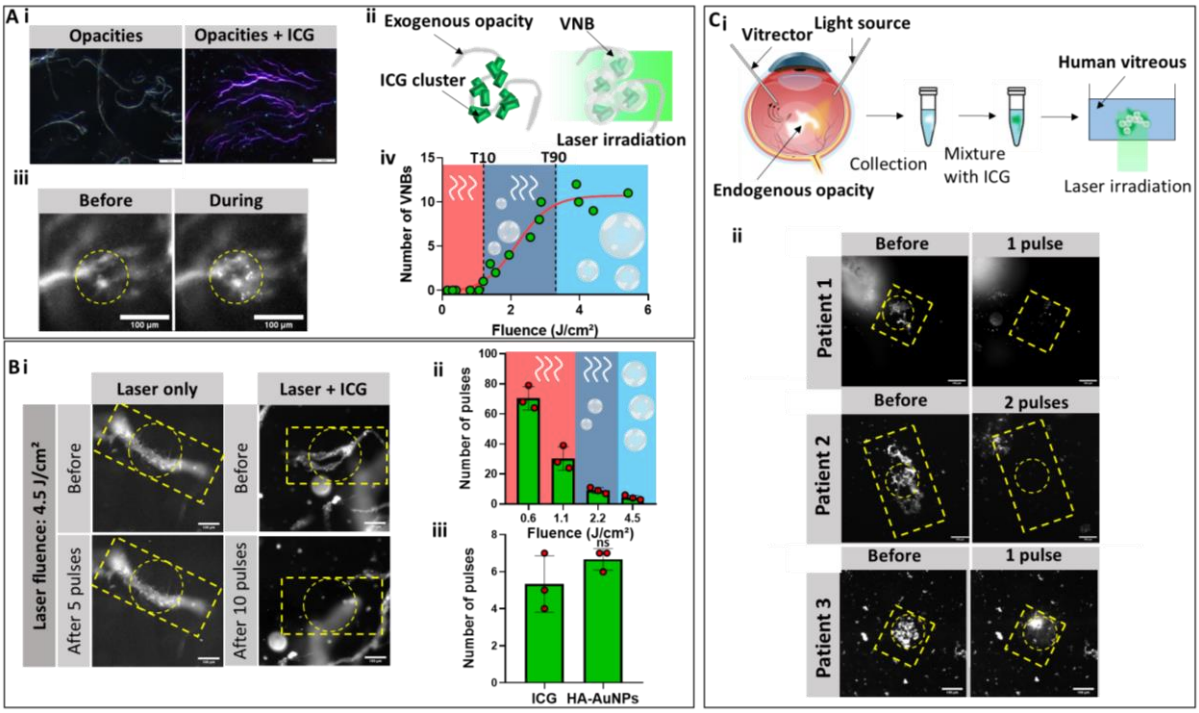

205

206 **Figure 3**. (A) (i) Dark field imaging of exogenous collagen opacities (0.02 mg/ml) in water,
207 before and after mixing with ICG (0.5 mg/ml); the scale bar is 100 µm. The presented images
208 are representative of 3 independent experiments. (ii) Illustration of ICG clustering on
209 collagenous structures and subsequent VNB generation upon laser irradiation. (iii) During
210 irradiation VNBs can be observed as bright spots at the surface of the collagen structures (4.5
211 J/cm²; 561 nm; <7 ns); the scale bar is 100 µm. The presented images are representative of 3
212 independent experiments. (iv) The number of VNBs generated at the surface of exogenous
213 collagen opacities (loaded with ICG) as a function of the laser fluence, following the application
214 of a single pulse[21,22]. For fluences lower than 0.1 J/cm² (T10), heat generation is predominant
215 (heating mode); between T10 and T90, both heat and bubbles are generated (intermediate
216 regime); for laser fluences higher than 3.3 J/cm² (T90), only VNBs are formed (bubble mode).
217 (B) (i) ICG (0.5 mg/ml) mixed with exogenous collagen opacities (0.02 mg/ml) locally generate
218 VNBs leading to the mechanical destruction of the opacities; the scale bar is 100 µm. See **Movie**
219 **1.** (ii) Destroying exogenous collagen in the heat mode, intermediate mode and bubble mode;
220 using a higher laser fluence lowers the number of pulses required to completely ablate the
221 collagen structure. (iii) Comparison between the number of pulses required to completely
222 destroy an exogenous collagen opacity treated with respectively ICG (0.5 mg/mL) or HA-
223 AuNPs (10 nm; 10^{12} NPs/mL) at a fluence of 4.5 J/cm². n=3 rabbits, data are presented as mean
224 ± s.d, student's *t* test (two-tailed), ns, not significant. (C) (i) After vitrectomy, excised human
225 vitreous opacities were mixed with ICG (0.5 mg/mL). (ii) Human vitreous opacities of several

patients could be ablated with laser irradiation (<7ns; 4.5 J/cm²; 561 nm). See **Movie 2**. The presented images are representative of 3 different patients.

VNBs generated from ICG ablate exogenous collagen opacities in vivo

In a first series of experiments, we prepared ICG-labeled exogenous collagen opacities by mixing collagen and free ICG (1.25 mg/mL in water). We then injected the labeled opacities in the eyes of rabbits. The first observation was that the intravitreally injected opacities could be easily imaged by PAM at 578 and 800 nm (**Figure 4Ai**; at 578 nm both blood vessels and ICG-labeled opacities could be detected while at 800 nm only the opacities could be observed). Next, we injected intravitreally exogenous collagen opacities (non-labeled) and 5 days later ICG (1.25 mg/mL) was injected. While the opacities could be observed by OCT, PAM imaging revealed that ICG co-localizes with the opacities (**Figure 4Aii**), confirming that intravitreally injected ICG could reach and bind to exogenous collagen opacities in the vitreous body.

As shown in **Figure 4Bii**, after intravitreal injection, ICG could be visualized by fundus imaging at all concentrations (0.25, 0.625 and 1.25 mg/ml). After one day, most of the injected ICG was no longer visible, most likely due to clearance from the vitreous body. Interestingly, when a sufficiently high ICG concentration was injected (i.e. 0.625 and 1.25 mg/ml), after 7 days ICG remained visible only at the level of the collagen opacity (**Figure 4Bii**).

Subsequently, we irradiated the exogenous collagen opacities with laser pulses. As shown in **Figure 4Biii**, applying laser pulses without the use of ICG did not destroy the opacities. However, following intravitreal injection of ICG (1.25 mg/mL), 5 laser pulses (i.e., 5 scans; 1.9 J/cm²) were sufficient to completely ablate injected collagen opacities (**Figure 4Biv**). Since retinal toxicity might be observed at high ICG concentration[38], we investigated a lower concentration (0.625 mg/mL) and still saw ablation of collagen opacities (**Figure 4Biv**), demonstrating that ICG has the capacity to destroy exogenous collagen opacities *in vivo* using laser settings (i.e., number of pulses (scans), laser fluence) similar to those used with HA-AuNPs (**Figure 2Cv**), and at an ICG concentration which is lower than the one clinically used for ILM chromodissection (usually between 1 and 5 mg/mL)[39]. On all rabbits tested (n=3), 3.3 +/-1.5 pulses seemed sufficient to destroy the intravitreally injected opacities.

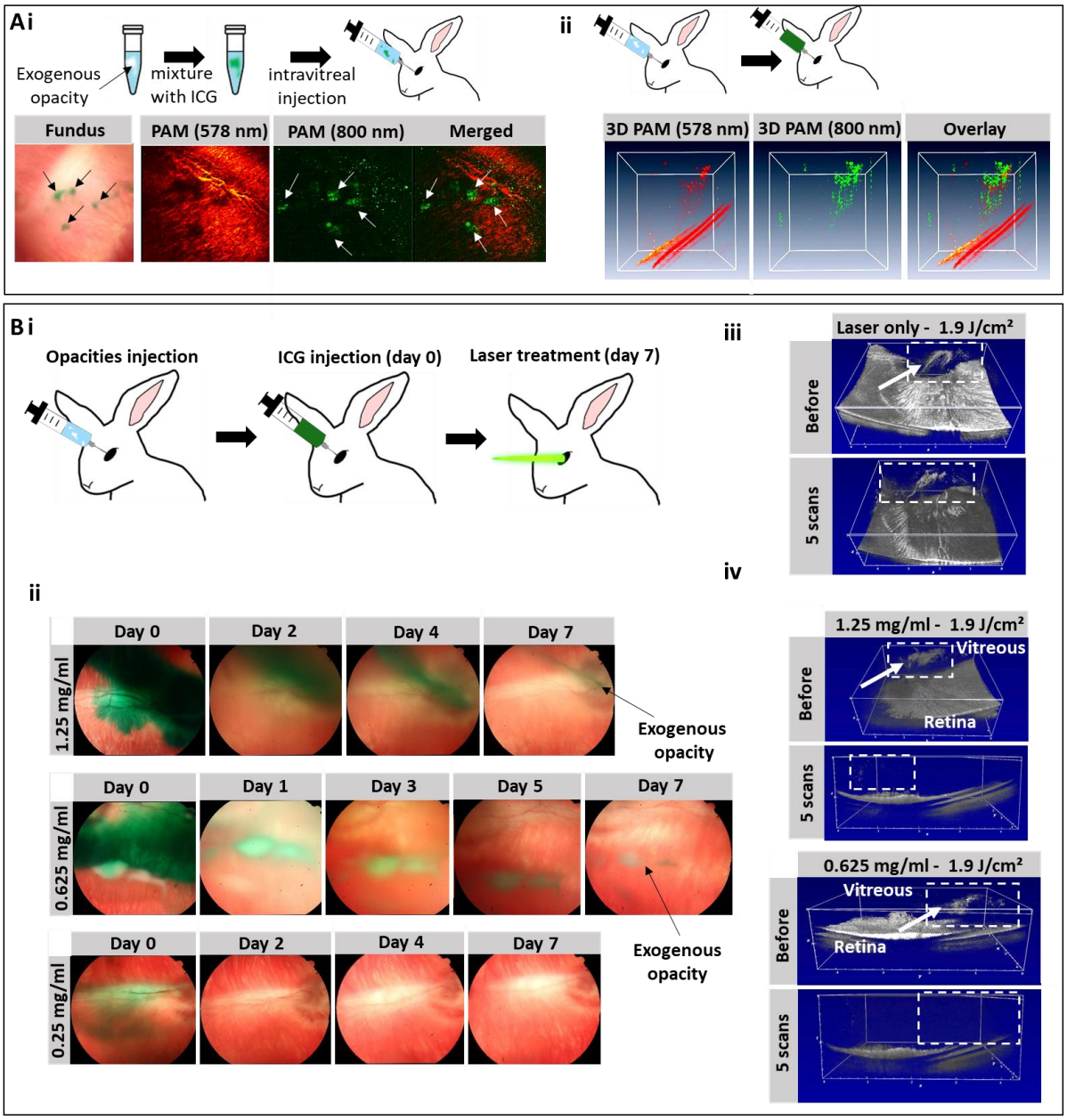

Figure 4. (A) (i) Intravitreally injected ICG-labeled exogenous collagen opacities can be observed by fundus imaging and PAM; 578 nm images the retinal blood vessels while 800 nm detects ICG; (ii) ICG (1.25 mg/mL) injected in the vitreous of rabbits binds to exogenous collagen opacities and allows their observation with PAM-imaging. (B) (i,ii) Intravitreally injected ICG diffuses away from the injection site and is progressively cleared from the vitreous body. After 7 days, ICG was only detectable at the level of the exogenous collagen opacities, if a sufficiently high ICG concentration is used. (iii) 2D OCT image of an injected exogenous collagen opacity (indicated by the white arrow) treated with a pulsed laser (5 pulses (scans); <7 ns; 800 nm; 1.9 J/cm²) without the injection of ICG. A region of interest (4.5×4.5 mm²,

containing the injected exogenous collagen opacities) was scanned with the laser (white dotted rectangle). (iv) Following ICG injection (1.25 and 0.625 mg/mL), laser irradiation (<7ns; 800 nm; 1.9 J/cm²) enabled the ablation of exogenous collagen opacities (5 pulses). The presented images in this figure are representative of images obtained in 3 rabbits.

Nanobubble ablation is safe to use in the rabbit eye

Visual inspection revealed that eyes treated with laser (with and without ICG or HA-AuNPs) showed normal anterior segments. Fundus imaging demonstrated no posterior segment abnormalities. OCT imaging revealed normal retinal anatomy (**Figure S3**).

Electroretinography waveforms did not show significant differences between untreated and treated rabbits **(Figure 5Ai** and **Figure S4)**. The mean amplitude (which reflects the health of the inner retinal layers) and the implicit time of b-wave (which is the time from the flash onset to the peak of the b-wave) showed a slight reduction for all responses obtained in the treated groups. The fluctuation rate (i.e., variation of responses within the same group) was approximately 16% for ICG + laser, 13% for HA-AuNPs + laser and 6% for laser only (**Figures 5Aii, 5Aiii**). For all the treatment conditions, the implicit time was not significantly different from the control group (n=3, P values＞0.05). Similarly, the average amplitude and implicit time of b-wave in scotopic combined rod and cone response and photopic b-wave fluctuated slightly between the treated groups without showing significant difference with the control group (**Figure S4**).

As **Figure 5B** shows there were no differences in the structure and thickness of the retina among the four groups (**Figure S3B and C**), and changes in cell morphology were not observed. TUNEL staining (**Figure 5B,** third row) found no evidence of apoptosis.

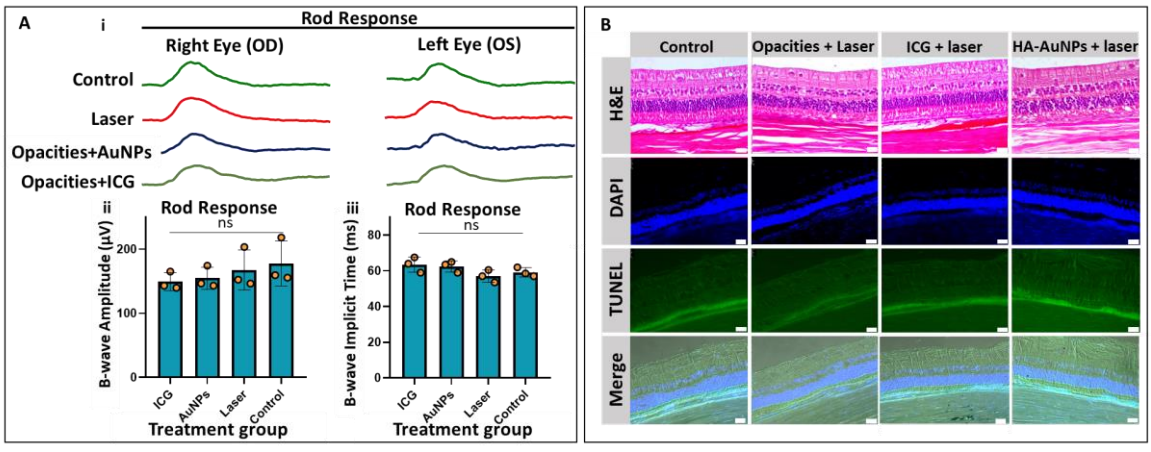

Figure 5. (A) Representative electroretinograms (ERGs). (i) Rod-isolated ERG waveforms. (ii) Comparison of the average ERG amplitudes between the four groups (<7ns, 1.9 J/cm²; ICG 0.625 mg/ml, 5 pulses at 800 nm; HA-AuNPs 10^{12} NPs/ml, 7 pulses at 532 nm), demonstrating minimal fluctuation in amplitudes in all treated groups that is not statistically significant. (iii) Average rod implicit time of ERGs did not change significantly (n=3 rabbits, data are presented as mean ± s.d, student's *t* test (two-tailed), ns, not significant). (B) Histological analysis of the retina of rabbits which were euthanized 30 days after treatment; H&E sand TUNEL staining. The green fluorescent color indicates the TUNEL-positive cells detected in each group. Blue fluorescent color shows cell nuclei stained with DAPI. Scale bar = 25 µm. The presented images are representative of 3 rabbits for each group.

Conclusions

This investigation reveals that nanobubble-mediated ablation is a highly promising approach to destroy vitreous opacities that arise with aging and disease. Both HA-AuNPs and ICG are highly attractive for this purpose, as they spontaneously accumulate on vitreous opacities upon intravitreal injection. Applying a few nanosecond laser pulses of low energy (about 1000 times weaker than currently employed in clinical YAG laser therapy) generates localized vapor nanobubbles which mechanically destroy collagenous aggregates. Interestingly, the capacity of HA-AuNPs and ICG to destroy exogenous collagen structures and human vitreous opacities seemed highly similar while retinal toxicity in treated rabbits was not observed. Finally, pulsed lasers have been used in the anterior segment, but safety concerns have limited use within the posterior segment of the eye. Thus strategies that significantly lower the energy levels are required to avoid cavitation phenomena and subsequent photomechanical damages[17]. Importantly, both ICG and HA-AuNPs enabled ablation of opacities in the vitreous body at a light dose significantly lower than that currently employed clinically with YAG laser[16]. Using VNBs, only a few laser pulses around 10^{-2} mJ were sufficient, which we estimate to represent a (total) dose that is one thousand to one million times less than currently employed in clinical YAG laser therapy. This tremendous reduction of required light energy will make floater treatment much safer even making possible the treatment of opacities located close to the retina.

Some challenging questions remain for the translation of nanobubble-mediated ablation of vitreous opacities into the clinic. Firstly, since there is currently no model to induce endogenous vitreous opacities in animals, difficulties remain to study nanobubble-mediated ablation of more complex opacities such as Weiss ring, which does not only consist of collagen but also of peripapillary glial tissue. Therefore, evaluation of the efficacy in humans suffering

from opacities in the vitreous will be a next step. Also, though topical administration (of drugs) is often hampered by corneal barriers,[40] and while the transport from the anterior into the posterior segment is rather limited, topical administration of the photosensitizer such as ICG or HA-AuNPs, thus avoiding intravitreal injections, would be highly valuable. Besides efficacy, the safety of nanobubble-mediated ablation of vitreous opacities will largely determine success in clinical practice. In this regard, understanding the way photosensitizers are cleared from the vitreous body (via the anterior and/or posterior routes)[41] and quantifying the intravitreal residence time of photosensitizers and their interactions with intraocular tissues is of great importance. It is also important to note that, besides opacities, local liquefied areas may be present in the vitreous. One could wonder whether ICG would not preferably accumulate in such liquefied zones which could influence the efficacy and safety of the treatment. However, ICG is a small molecule which is expected to freely diffuse (with a similar speed) in both gel and liquefied vitreous[42]. Therefore we do not expect ICG to be excluded (sterically) from the gel phase and concentrate in the liquefied regions. Also note that free (i.e. non-accumulated) ICG would not generate VNBs at laser fluences used to destroy the opacities, even not at a higher concentration of 1 mg/ml which is the maximal solubility of ICG in water. Thus, even in case a local increase in the concentration of free ICG would occur, no damage will be likely observed.

An intriguing question is whether the destruction of the opacities occurs through the collapse of *nano*sized (sub-micron) vapor bubbles. The generation of nanoscopic bubbles upon pulsed laser irradiation of plasmonic nanoparticles (such as AuNPs) has been studied for more than a decade[43]. Many groups and ours based their rationale on theoretical modeling[44]. Also experimental attempts were made to measure the size of VNBs generated upon pulsed laser irradiation of plasmonic nanoparticles, though it is admitted by physicists that such measurements remain rather difficult considering the small size and short lifespan of the bubbles[45]. To date, VNB formation and cavitation phenomena from pulsed laser irradiation of ICG have not been reported. The physics of this newly observed phenomenon has not been studied so far and go beyond the aim of this work. Since we observed the formation of short-lived bubbles in dark field images, similar to what we observed for AuNPs, we hypothesized that laser irradiation of ICG at the surface of the opacities leads to the formation of vapor bubbles with a diameter below 1 µm, next to larger bubbles which are formed upon merging of adjacent nanobubbles. This hypothesis was confirmed by measuring the photo-acoustic signals during the laser irradiation of the opacities in the vitreous of rabbits treated with AuNPs or ICG

(**Figure S5)**. Our results were consistent with previous studies from us and others measuring PA signals of VNBs showing a lifespan of a few hundreds of nanoseconds[21,46].

In 2018, Palanker highlighted in the *New England Journal of Medicine:* "a potential future for the application of ultrafast lasers beyond the anterior chamber of the eye lies in the dissection of vitreous floaters"[47]. We believe that nanobubble ablation of vitreous opacities meets this need and will pave the way for a safe use of pulsed lasers in the posterior segment of the eye.

Acknowledgements

This research was supported by the Research Foundation Flanders (FWO, 12X3222N, FS).

Author contributions

F.S., K.B. and S.C.D.S conceived the concept of nanobubble ablation of vitreous opacities. F.S., V.V., R.X.and A.H. performed and analyzed the *in vitro/ex vivo* experiments. R.X. and K.B. designed the optical setup. J.S. contributed to the writing of the manuscript and performed vitrectomies. J.C.F. synthesized and characterized the gold nanoparticles. P.N and Y.L performed the experiments in rabbits. F.S., P.N and Y.L performed the analysis of the experiments in rabbits (OCT, PAM, histology and ERG). F.S., S.C.D, P.N and Y.P. designed the *in vivo* experiments. K.R., D.R., M.T., K.P., K.B., J.S., Y.P, A.H. and S.C.D advised and provided guidance on experiments and data analysis. All authors discussed the experimental results and jointly wrote the manuscript.

Competing interests

The authors declare no competing financial interests.

Additional information

Supplementary information is available for this paper.

Figure legends

Figure 1. (A) Vitreous liquefaction (i) is due to a progressive dissociation of HA from the collagen fibrils (ii, iii) leading to the aggregation of the fibrils forming increasingly large vitreous opacities (iii)[2,4,26]. We previously showed *ex vivo* that coating AuNPs with HA targets vitreous opacities which are largely devoid of HA (iii). Upon irradiation with a pulsed laser, VNBs formed and then collapsed, mechanically destroying the opacities[28]. (B) We hypothesize that indocyanine green (ICG; (i)) that is known to bind to collagen will 'cluster' on vitreous

opacities (ii, iii) and that subsequent laser irradiation of ICG will generate VNBs (preferentially) ablating the opacities. This should result in targeted 'nanobubble-mediated' ablation of the opacities (iv), leaving the surrounding vitreous untouched.

Figure 2. (A) HA-coated gold nanoparticles were found to accumulate on exogenous collagen opacities and human vitreous opacities obtained by vitrectomy in patients suffering from eye floaters. In (i) the red dotted lines represent the edges of an exogenous collagen opacity loaded with HA-coated gold nanoparticles (black dots). (ii, iii) Pulsed laser irradiation – *ex vivo* - of an exogenous collagen opacity (ii) and a human vitreous opacity (iii) ablates them (with permission from [28], Copyright 2019, ACS publications). The presented images are representative of 3 independent experiments. (B) The 'eye floater model' in rabbits: collagen opacities were prepared *in vitro* (named exogenous collagen opacities) and injected intravitreally in anesthetized rabbits. OCT confirmed that exogenous collagen opacities were present close to the retina (distances to the retina are indicated). (C) (i) HA-AuNPs were IVIT injected 5 days after IVIT injection of the exogenous collagen opacities and eyes were treated with laser (532 nm; 1.9 J/cm²) 3 days later; (ii) Areas in the vitreous body of anesthetized rabbits (4.5×4.5 mm²) were scanned with the laser beam. (iii) Fundus observations revealed reddish collagen opacities (dotted white circle) suggesting accumulation of HA-AuNPs on the opacities, which was confirmed by PAM-imaging (iv; 578 nm). (v) OCT imaging revealed that pulsed laser irradiation destroyed the exogenous collagen opacities; after 7 laser pulses (scans) the collagen opacities were gone. For all the rabbits (n=3) we observed that 5 ± 2 (mean ± s.d.) pulses were sufficient to completely ablate the opacities.

Figure 3. (A) (i) Dark field imaging of exogenous collagen opacities (0.02 mg/ml) in water, before and after mixing with ICG (0.5 mg/ml); the scale bar is 100 µm. The presented images are representative of 3 independent experiments. (ii) Illustration of ICG clustering on collagenous structures and subsequent VNB generation upon laser irradiation. (iii) During irradiation VNBs can be observed as bright spots at the surface of the collagen structures (4.5 J/cm²; 561 nm; <7 ns); the scale bar is 100 µm. The presented images are representative of 3 independent experiments. (iv) The number of VNBs generated at the surface of exogenous collagen opacities (loaded with ICG) as a function of the laser fluence, following the application of a single pulse[21,22]. For fluences lower than 0.1 J/cm² (T10), heat generation is predominant (heating mode); between T10 and T90, both heat and bubbles are generated (intermediate regime); for laser fluences higher than 3.3 J/cm² (T90), only VNBs are formed (bubble mode). (B) (i) ICG (0.5 mg/ml) mixed with exogenous collagen opacities (0.02 mg/ml) locally generate

VNBs leading to the mechanical destruction of the opacities; the scale bar is 100 µm. See **Movie 1.** (ii) Destroying exogenous collagen in the heat mode, intermediate mode and bubble mode; using a higher laser fluence lowers the number of pulses required to completely ablate the collagen structure. (iii) Comparison between the number of pulses required to completely destroy an exogenous collagen opacity treated with respectively ICG (0.5 mg/mL) or HA-AuNPs (10 nm; 10^{12} NPs/mL) at a fluence of 4.5 J/cm². (C) (i) After vitrectomy, excised human vitreous opacities were mixed with ICG (0.5 mg/mL). (ii) Human vitreous opacities of several patients could be ablated with laser irradiation (<7ns; 4.5 J/cm²; 561 nm). See **Movie 2**. The presented images are representative of 3 different patients.

Figure 4. (A) (i) Intravitreally injected ICG-labeled exogenous collagen opacities can be observed by fundus imaging and PAM; 578 nm images the retinal blood vessels while 800 nm detects ICG; (ii) ICG (1.25 mg/mL) injected in the vitreous of rabbits binds to exogenous collagen opacities and allows their observation with PAM-imaging. (B) (i,ii) Intravitreally injected ICG diffuses away from the injection site and is progressively cleared from the vitreous body. After 7 days, ICG was only detectable at the level of the exogenous collagen opacities, if a sufficiently high ICG concentration is used. (iii) 2D OCT image of an injected exogenous collagen opacity (indicated by the white arrow) treated with a pulsed laser (5 pulses (scans); <7 ns; 800 nm; 1.9 J/cm²) without the injection of ICG. A region of interest (4.5×4.5 mm², containing the injected exogenous collagen opacities) was scanned with the laser (white dotted rectangle). (iv) Following ICG injection (1.25 and 0.625 mg/mL), laser irradiation (<7ns; 800 nm; 1.9 J/cm²) enabled the ablation of exogenous collagen opacities (5 pulses). The presented images in this figure are representative of images obtained in 3 rabbits.

Figure 5. (A) Electroretinograms (ERGs). (i) Rod-isolated ERG waveforms. (ii) Comparison of the average ERG amplitudes between the four groups (<7ns, 1.9 J/cm²; ICG 0.625 mg/ml, 5 pulses at 800 nm; HA-AuNPs 10^{12} NPs/ml, 7 pulses at 532 nm), demonstrating minimal fluctuation in amplitudes in all treated groups that is not statistically significant. (iii) Average rod implicit time of ERGs did not change significantly (n=3 rabbits, data are presented as mean ± s.d, student's *t* test (two-tailed), ns, not significant). (B) Histological analysis of the retina of rabbits which were euthanized 30 days after treatment; H&E sand TUNEL staining. The green fluorescent color indicates the TUNEL-positive cells detected in each group. Blue fluorescent color shows cell nuclei stained with DAPI. Scale bar = 25 µm. The presented images are representative of 3 rabbits for each group.

Data availability statement

All data supporting the findings of this study are available within the paper and its Supplementary Information. Source data are provided with this paper. Any further related information can be provided by the corresponding author upon reasonable request.

References

1. Chiti, F. & Dobson, C. M. Protein Misfolding, Functional Amyloid, and Human Disease. *Annu. Rev. Biochem.* **75**, 333–366 (2006).

2. Sebag, J. Vitreous and Vision Degrading Myodesopsia. *Prog. Retin. Eye Res.* 100847 (2020) doi:10.1016/j.preteyeres.2020.100847.

3. Asakura, A. [Histochemistry of hyaluronic acid of the bovine vitreous body by electronmicroscopy]. *Nippon Ganka Gakkai Zasshi* **89**, 179–191 (1985).

4. Sebag, J. & Balazs, E. A. Morphology and ultrastructure of human vitreous fibers. *Invest. Ophthalmol. Vis. Sci.* **30**, 1867–1871 (1989).

5. Sebag, J. Floaters and the quality of life. *Am. J. Ophthalmol.* **152**, 3-4.e1 (2011).

6. Webb, B. F., Webb, J. R., Schroeder, M. C. & North, C. S. Prevalence of vitreous floaters in a community sample of smartphone users. *Int. J. Ophthalmol.* **6**, 402–405 (2013).

7. Zou, H., Liu, H., Xu, X. & Zhang, X. The impact of persistent visually disabling vitreous floaters on health status utility values. *Qual. Life Res.* **22**, 1507–1514 (2013).

8. Wagle, A. M., Lim, W.-Y., Yap, T.-P., Neelam, K. & Au Eong, K.-G. Utility values associated with vitreous floaters. *Am. J. Ophthalmol.* **152**, 60-65.e1 (2011).

9. Kim, Y.-K. *et al.* Psychological Distress in Patients with Symptomatic Vitreous Floaters. *Journal of Ophthalmology* https://www.hindawi.com/journals/joph/2017/3191576/ (2017) doi:https://doi.org/10.1155/2017/3191576.

10. Milston, R., Madigan, M. C. & Sebag, J. Vitreous floaters: Etiology, diagnostics, and management. *Surv. Ophthalmol.* **61**, 211–227 (2016).

11. Sebag, J., Yee, K. M. P., Wa, C. A., Huang, L. C. & Sadun, A. A. Vitrectomy for floaters: prospective efficacy analyses and retrospective safety profile. *Retina Phila. Pa* **34**, 1062–1068 (2014).

12. Macherner, R. The development of pars plana vitrectomy: a personal account. *Graefes Arch. Clin. Exp. Ophthalmol.* **233**, 453–468 (1995).

13. Holekamp, N. M., Shui, Y.-B. & Beebe, D. C. Vitrectomy surgery increases oxygen exposure to the lens: A possible mechanism for nuclear cataract formation. *Am. J. Ophthalmol.* **139**, 302–310 (2005).

14. Kunimoto, D. Y. & Kaiser, R. S. Incidence of Endophthalmitis after 20- and 25-Gauge Vitrectomy. *Ophthalmology* **114**, 2133–2137 (2007).

15. Tsai, W. F., Chen, Y. C. & Su, C. Y. Treatment of vitreous floaters with neodymium YAG laser. *Br. J. Ophthalmol.* **77**, 485–488 (1993).

16. Procedure Guide: Vitreous Opacities - Ellex. https://www.ellex.com/resources/procedure-guide-vitreous-opacities/.

17. Rockwell, B. A., Thomas, R. J. & Vogel, A. Ultrashort laser pulse retinal damage mechanisms and their impact on thresholds. *Med. Laser Appl.* **25**, 84–92 (2010).

18. Delaney, Y. M., Oyinloye, A. & Benjamin, L. Nd:YAG vitreolysis and pars plana vitrectomy: surgical treatment for vitreous floaters. *Eye* **16**, 21–26 (2002).

19. Koo, E. H., Haddock, L. J., Bhardwaj, N. & Fortun, J. A. Cataracts induced by neodymium–yttrium-aluminium-garnet laser lysis of vitreous floaters. *Br. J. Ophthalmol.* **101**, 709–711 (2017).

20. Xiong, R., Xu, R. X., Huang, C., Smedt, S. D. & Braeckmans, K. Stimuli-responsive nanobubbles for biomedical applications. *Chem. Soc. Rev.* (2021) doi:10.1039/C9CS00839J.

21. Xiong, R. *et al.* Comparison of Gold Nanoparticle Mediated Photoporation: Vapor Nanobubbles Outperform Direct Heating for Delivering Macromolecules in Live Cells. *ACS Nano* **8**, 6288–6296 (2014).

22. Liu, J. *et al.* Repeated photoporation with graphene quantum dots enables homogeneous labeling of live cells with extrinsic markers for fluorescence microscopy. *Light Sci. Appl.* **7**, 47 (2018).

23. Harizaj, A. *et al.* Photoporation with Biodegradable Polydopamine Nanosensitizers Enables Safe and Efficient Delivery of mRNA in Human T Cells. *Adv. Funct. Mater.* **n/a**, 2102472.

24. Barras, A. *et al.* Carbon quantum dots as a dual platform for the inhibition and light-based destruction of collagen fibers: implications for the treatment of eye floaters. *Nanoscale Horiz.* (2021) doi:10.1039/D1NH00157D.

25. Hua, D. *et al.* Bubble Forming Films for Spatial Selective Cell Killing. *Adv. Mater. Deerfield Beach Fla* e2008379 (2021) doi:10.1002/adma.202008379.

26. Ueno, N., Sebag, J., Hirokawa, H. & Chakrabarti, B. Effects of visible-light irradiation on vitreous structure in the presence of a photosensitizer. *Exp. Eye Res.* **44**, 863–870 (1987).

27. Filas, B. A., Zhang, Q., Okamoto, R. J., Shui, Y.-B. & Beebe, D. C. Enzymatic degradation identifies components responsible for the structural properties of the vitreous body. *Invest. Ophthalmol. Vis. Sci.* **55**, 55–63 (2014).

28. Sauvage, F. *et al.* Photoablation of Human Vitreous Opacities by Light-Induced Vapor Nanobubbles. *ACS Nano* **13**, 8401–8416 (2019).

29. Ziefuss, A. R., Reich, S., Reichenberger, S., Levantino, M. & Plech, A. In situ structural kinetics of picosecond laser-induced heating and fragmentation of colloidal gold spheres. *Phys. Chem. Chem. Phys.* **22**, 4993–5001 (2020).

30. Pan, Y. *et al.* Size-Dependent Cytotoxicity of Gold Nanoparticles. *Small* **3**, 1941–1949 (2007).

31. Desmettre, T., Devoisselle, J. M. & Mordon, S. Fluorescence Properties and Metabolic Features of Indocyanine Green (ICG) as Related to Angiography. *Surv. Ophthalmol.* **45**, 15–27 (2000).

32. Burk, S. E., Da Mata, A. P., Snyder, M. E., Rosa, R. H. & Foster, R. E. Indocyanine green-assisted peeling of the retinal internal limiting membrane. *Ophthalmology* **107**, 2010–2014 (2000).

33. Seitz, B. & Langenbucher, A. Lasers in ophthalmology. *The Lancet* **356**, S26 (2000).

34. Masse, F., Ouellette, M., Lamoureux, G. & Boisselier, E. Gold nanoparticles in ophthalmology. *Med. Res. Rev.* **39**, 302–327 (2019).

35. Pereira, D. V. *et al.* Effects of Gold Nanoparticles on Endotoxin-Induced Uveitis in Rats. *Invest. Ophthalmol. Vis. Sci.* **53**, 8036–8041 (2012).

36. Chen, F., Si, P., Zerda, A. de la, V. Jokerst, J. & Myung, D. Gold nanoparticles to enhance ophthalmic imaging. *Biomater. Sci.* **9**, 367–390 (2021).

37. Hayashi, A., Naseri, A., Pennesi, M. E. & de Juan, E. Subretinal delivery of immunoglobulin G with gold nanoparticles in the rabbit eye. *Jpn. J. Ophthalmol.* **53**, 249–256 (2009).

38. Rodrigues, E. B., Meyer, C. H., Mennel, S. & Farah, M. E. Mechanisms of intravitreal toxicity of indocyanine green dye: implications for chromovitrectomy. *Retina Phila. Pa* **27**, 958–970 (2007).

39. Kwok, A. K. H., Lai, T. Y. Y., Yew, D. T. W. & Li, W. W. Y. Internal limiting membrane staining with various concentrations of indocyanine green dye under air in macular surgeries. *Am. J. Ophthalmol.* **136**, 223–230 (2003).

40. Wels, M., Roels, D., Raemdonck, K., De Smedt, S. C. & Sauvage, F. Challenges and strategies for the delivery of biologics to the cornea. *J. Controlled Release* **333**, 560–578 (2021).

41. Del Amo, E. M. *et al.* Pharmacokinetic aspects of retinal drug delivery. *Prog. Retin. Eye Res.* **57**, 134–185 (2017).

42. Käsdorf, B. T., Arends, F. & Lieleg, O. Diffusion Regulation in the Vitreous Humor. *Biophys. J.* **109**, 2171–2181 (2015).

43. Lapotko, D. Optical excitation and detection of vapor bubbles around plasmonic nanoparticles. *Opt. Express* **17**, 2538–2556 (2009).

44. Xiong, R. *et al.* Laser-assisted photoporation: fundamentals, technological advances and applications. *Adv. Phys. X* **1**, 596–620 (2016).

45. Lukianova-Hleb, E. *et al.* Plasmonic Nanobubbles as Transient Vapor Nanobubbles Generated around Plasmonic Nanoparticles. *ACS Nano* **4**, 2109–2123 (2010).

46. Lukianova-Hleb, E. Y. *et al.* Hemozoin-generated vapor nanobubbles for transdermal reagent- and needle-free detection of malaria. *Proc. Natl. Acad. Sci.* **111**, 900–905 (2014).

47. Palanker, D. Femtosecond Lasers for Ophthalmic Surgery Enabled by Chirped-Pulse Amplification. *N. Engl. J. Med.* **379**, 2267–2269 (2018).

Methods

1. Chemicals

Hyaluronic acid 20 kDa (HA; Invitrogen), indocyanine green (ICG) (Sigma-Aldrich), rat tail collagen type I acid solution (Sigma-Aldrich), ethanol (Chem-Lab NV).

2. Synthesis and characterization of HA-AuNPs

The synthesis and HA-coating of 10 nm AuNPs were performed as previously reported[48]. Briefly, $HAuCl_4$ (in water) and sodium ascorbate (in water) were mixed at equimolar ratios (concentration 0.2 mM, final volume 100 mL). We allowed the reaction to proceed until the UV−vis extinction spectrum of 10 nm AuNPs was observed. NPs were then washed by centrifugation (10 min at 13000 g). Coating with HA was performed by adding 1 mL of an HA-solution (3 mg HA/mL in distilled deionized water) to 50 mL of a AuNP dispersion in water (2−4 pM). HA-coated AuNPs were finally washed by centrifugation, resuspended in water, and stored at 4°C for further use. The synthetized HA-AuNPs were characterized by dynamic light scattering and zeta potential measurements. The concentration of the AuNPs in the dispersions (i.e., number of AuNPs per mL) was estimated by nanoparticle tracking analysis (NTA) using a Nanosight instrument (Malvern), as previously reported[48].

3. Laser-induced formation of vapor bubbles (VNBs) and VNB threshold

To evaluate whether ICG generates VNBs, ICG solutions were irradiated with a pulsed nanosecond laser (HE 355 LD laser, OPOTEK Inc.; 7 ns, 561 nm). Note that VNBs can be easily visualized by dark-field microscopy as they scatter light. Dark-field images were recorded before and during irradiation of free ICG in water and free ICG mixed with collagen using laser pulses with a varying fluence, respectively. The ‘VNB threshold’ (T90) for ICG and HA AuNPs, which is the fluence of a single laser pulse at which 90% of the irradiated particles generate a VNB, was determined by plotting the number of bubbles as a function of the laser fluence.

4 In vitro and ex vivo photo-ablation of exogenous collagen opacities and human vitreous opacities

4.1 Exogenous collagen opacities

Exogenous collagen opacities were prepared from type I collagen (rat tails) as reported previously[48]. Collagen I was dissolved in PBS (0.2 mg/ mL); the pH of the collagen solution

was increased to 7.4 with NaOH (0.1 N). The collagen solution was then incubated at 37 °C for 1 h. To follow the collagen fibrillation process, turbidity experiments were performed by measuring the absorbance of the collagen suspension (λ 300 nm) at 37 °C (using a NanoDrop 2000c spectrophotometer).

4.2 Human vitreous opacities

Human vitreous opacities were collected from patients undergoing vitrectomy (JS). IRB-approved informed consent was obtained and undiluted samples were frozen at −80°C.

4.3 Mixing exogenous collagen opacities and human vitreous opacities with HA-AuNPs or ICG

Suspensions of exogenous collagen opacities (0.2 mg/ml) were mixed with either ICG (dissolved in water) or HA-AuNPs (dispersed in water); after mixing, the concentration of collagen was 0.02 mg/ml, while the concentration of ICG and HA-AuNPs equaled 0.5 mg/ml and 10^{12} NPs/ml, respectively. Samples containing human vitreous opacities were diluted one-to-one (v/v) with a solution of free ICG (1 mg/mL in water), so that the final ICG concentration was 0.5 mg/ml.

4.4 Laser treatment of exogenous collagen opacities and human vitreous opacities (in vitro / ex vivo)

Samples of either exogenous collagen opacities or human vitreous opacities treated with ICG or HA-AuNPs (see 2.4.3) were placed on a glass bottom dish and covered with a cover glass before irradiation. Dark-field microscopy was performed to focus the nanosecond laser on the exogenous collagen opacities/human vitreous opacities in the samples. Samples were then illuminated with laser pulses (wavelength=561 nm, pulse duration < 7 ns). A beam expander (#GBE05-A, Thorlabs) combined with iris diaphragm (#D37SZ, Thorlabs) was used to adjust the diameter of the laser beam to 150 µm. The laser pulse energy was monitored by an energy meter (J-25MB-HE&LE, Energy Max-USB/RS sensors, Coherent) synchronized with the pulsed laser. The set-up was made in such way that we could illuminate the sample pulse by pulse and record images during illumination with NIS software (Nikon).

5 In vivo imaging and nanobubble ablation of exogenous collagen opacities

5.1 Animal preparation

All animal experiments were performed under the guidelines of the Association for Research in Vision and Ophthalmology (ARVO). Experimental protocols were approved by

624 the Institutional Animal Care and Use Committee (IACUC) of the University of Michigan
625 (Protocol PRO00008566, PI Paulus). A total of 18 New Zealand White rabbits (age 3–6 months;
626 weight 2.45–3.15 kg; both genders) were randomly divided into 6 groups: control group A
627 treated with laser only (N=3), group B received an intravitreal injection of ICG (N=3), group C
628 an intravitreal injection of ICG labeled exogenous collagen opacities (N=3), group D with
629 exogenous collagen opacities followed by intravitreal injection of ICG (N=3), group E with
630 HA-AuNPs labeled exogenous collagen opacities (N=3), and group F was injected with
631 exogenous collagen opacities followed by intravitreal injection of HA-AuNPs (N=3). During
632 the *in vivo* experiments, animal conditions such as mucous membrane color, heart rate, body
633 heat, and respiratory rate were monitored every 15 minutes. Animals were anesthetized with
634 intramuscular ketamine (40 mg/kg) and xylazine (5 mg/kg). Tropicamide (1%) and
635 phenylephrine hydrochloride (2.5%) were used to dilate pupils for imaging. For topical
636 anesthesia, tetracaine (0.5%) was used. To avoid corneal dehydration a lubricant (Systane,
637 Alcon Inc.) was applied every minute. To maintain anesthesia, a dose of ketamine (13 mg/kg)
638 was injected every 45 min. The animal's body heat was maintained using a circulating heat
639 blanket.

640 *5.2 Intravitreal injections*

641 To visualize the fundus, a microscope and plastic contact lens were used to target a
642 location in the vitreous body for injection with a 27-gauge needle. In one series of experiments
643 40 µL of exogenous collagen opacities pre-treated with either HA-AuNPs or ICG (see section
644 2.4.3) were injected; the concentration of collagen in the dispersions was 0.02 mg/ml. In another
645 series of experiments, 40 µL of exogenous collagen opacities (0.02 mg/ml) were injected
646 intravitreally, followed 5 days later by injection of 40 µL of ICG (0.25-1.25 mg/ml) or HA-
647 AuNPs (10^{12} NPs/ml). The position of the exogenous collagen opacities in the vitreous body
648 was monitored by optical coherence tomography (OCT) so that the intravitreal injection of ICG
649 or HA-AuNPs could be performed close to the area where the opacities were located. Three
650 days after the injection of ICG or HA-AuNPs, laser treatment was performed as reported in
651 section 2.5.4.

652 *5.3 Color fundus photography, fluorescence imaging, PAM- and OCT-imaging*

653 Rabbits were monitored one minute after intravitreal injection of the exogenous collagen
654 opacities and at day 4 post intravitreal injection of ICG or HA-AuNPs. Rabbits intravitreally
655 injected with ICG and HA-AuNPs only were followed up for 14 days post injection. The rabbit

eyes were assessed by color fundus photography, fluorescence imaging, optical coherence tomography (OCT) and photoacoustic microscopy (PAM), as described below. The same scanning areas for PAM- and OCT-imaging were monitored by the fundus camera which was integrated in the OCT system. To detect the photoacoustic signal, the ultrasound transducer was placed in contact with the conjunctiva, allowing it to move freely in 3D while not applying any physical pressure on the rabbit eyes. The scanning areas (i.e. areas containing the injected opacities) were selected by the fundus camera and captured by PAM.

Color fundus photography was performed using a 50-degree color fundus photography system (Topcon 50EX, Topcon Corporation, Tokyo, Japan). The fundus image was captured using an EOS 5D camera (resolution of 5472×3648 pixels with a pixel size of 6.55 μm^2; Canon, Japan). Several regions were imaged including the optic nerve, the retina above and below the optic disc, the temporal medullary ray and the nasal medullary ray. Fluorescence imaging was done with the Topcon 50EX system using appropriate excitation and emission filters.

PAM and OCT imaging used a custom-built integrated PAM and OCT system developed to track the location of the vitreous opacities, as shown in **Figure S6**. Briefly, for PAM, a tunable nanosecond pulsed laser produced by a solid-state Q-switched Nd:YAG laser (NT-242, Ekspla) was used as a light source. The optical wavelength could be adjusted (405 – 2600 nm), the pulse repetition rate was 1 kHz and the pulse duration 3–5 ns. The output laser light was spread through the iris, filtered and collimate to form a homogeneous beam size of 2 mm. Then, the laser light was passed through a galvanometer and telescope consisting in a scan lens and an ocular lens and focused on the fundus of the retina with an estimated diameter of 20 µm. To detect the photoacoustic (PA) signal, a customized needle-shaped ultrasound transducer was used (center frequency of 27 MHz, two-way bandwidth -60%, Optosonic Inc., Arcadia, CA, USA). The detected PA signals were amplified using a 1.4 dB preamplifier (AU-1647, L3 Narda-MITEQ). Then, the analog data were converted into digital signals and digitized at a sampling rate of 500 MHz using a DAQ card (PX1500-4, Signatec Inc.).

For PAM-imaging, light of 578 nm (to detect retinal and choroidal vessels) and 800 nm (to detect ICG) with an average energy of 80 nJ illuminated the eyes. This is about half of the maximal energy of a single laser pulse (~ 160 nJ at 570 and 800 nm) which might be applied to the retina, as defined by the American National Standards Institute (ANSI)[49]. By using the full-width at half-maximum (FWHM) of line spread functions (LSFs) and A-line signal (one-dimensional point spread function), the lateral and axial resolution equaled 4.1 µm and 37.0

μm, respectively. Both 2D and 3D PAM-images could be obtained with an acquisition time of 65 s by using an optical scanning galvanometer.

The OCT setup used in this study was built using a commercially available spectral domain Ganymede-II-HR OCT device (Thorlabs) to which a dispersion compensation glass and an ocular lens were added, as shown in **Figure S1**. To excite the sample, two super luminescent diodes with central wavelengths of 846 nm and 932 nm were used. The incident light beam was coaxially aligned with the PAM laser beam, allowing to obtain both PAM and OCT at the same location and co-registering the OCT and PAM-images on the same orthogonal imaging plane. The OCT lateral and axial resolutions were 3.8 μm and 4.0 μm, respectively. A cross-sectional B-scan OCT image can be obtained within 0.103 seconds with a resolution of 512×1024 A-lines at the scanning rate of 36 kHz. 3D volumetric OCT images with a volume of 4.5×4.5×1.8 mm^3 (512×512×1024 pixels) were obtained within 2 min (with average rate of 3 times).

5.4 Laser treatment of rabbit eyes in vivo

Anesthetized rabbits were kept on a custom-built stabilization platform. After imaging and localizing opacities, regions in the eyes (4.5×4.5 mm^2) were illuminated with laser pulses (< 7 ns; 1.9 J/cm^2; NT-242, Ekspla) of 532 nm (HA-AuNPs) or 800 nm (ICG) to treat the exogenous vitreous opacities (**Figure S6**); the step size of the scanning laser was 9 μm, the beam size equaled 20 μm. During the treatment, real-time OCT was active to monitor the position of the exogenous collagen opacities. The 4.5×4.5 mm^2 area was laser scanned several times (3-7 times) until the opacities could no longer be visualized. After the laser treatment, PAM and fundus images were performed to evaluate the potential damage to retinal vessels. Also, rabbit vital signs were monitored and recorded until the animals fully recovered from anesthesia.

5.5 In vivo safety evaluation

Treated eyes were examined after the laser treatment and again at 1 month: anterior structures using slit lamp bio-microscopy (SL120, Carl Zeiss, Germany); posterior structures using a contact fundus lens (Volk Optical Inc.).

5.6 Electroretinography (ERG)

Full field electroretinography (ff-ERG) was performed before and 30 days after laser treatment. Pupils were dilated and rabbits were maintained in a dark room for 1 hour, then anesthetized. To avoid corneal dehydration, a lubricant gel (Gonak, Akorn Inc.) was used upon

positioning of the ERG-Jet contact lens electrodes (The Electrode Store) on the cornea. Two reference needle electrodes were inserted subcutaneously behind both ears. A piece of ground electrode was placed in the scruff. The ERG (LKC UTAS 3000 electrophysiology system, LKC Technologies) was performed in a dark room to distinguish rod and cone response. Dark adaptation responses were amplified at 2500 gain at 0.3-500 Hz and digitized at a rate of 2000 Hz. Scotopic ERGs were obtained under excitation of flash light at intensity of 0.01 cd.s/m^2 for the rod isolated ERG and at 3.0 cd.s/m^2 for the combination of rod-cone ERG. Then, light adaptation was performed by maintaining the rabbits under flashlight with intensity of 32 cd/m^2 for 10 min. Photopic ERGs were acquired under the excitation of flashlight at an intensity of 3.0 cd.s/m^2. The ERG data was quantified from the acquired scotopic and photopic waveforms. The a-wave amplitude was calculated from the pre-stimulus baseline to the trough of the a-wave. The implicit time of the a-wave was determined from flash onset to the trough of the a-wave. The b-wave amplitude was isolated from the trough of the a-wave to the peak of the b-wave. The b-wave implicit time was measured from flash onset to the peak of the b-wave.

5.7 Histopathologic and TUNEL assays

To further assess safety of the laser treatment, rabbits were euthanized after 30 days, harvested, and fixed in Davidson's fixative solution (Electron Microscope Sciences) for 24 hours. The eyes were transferred to 50 % alcohol solution (Fisher Scientific) and kept at room temperature for 8 hours, then placed in 70 % alcohol at room temperature for 24h. The anterior segment and vitreous body were removed and the remaining tissues were fixed in 2% agarose prior to embedding in paraffin. Embedded tissues were sectioned 4 µm thick and stained with hematoxylin and eosin (H&E) for histology analysis using a Leica autostainer XL. Terminal deoxynucleotidyl transferase dUTP nick end labeling (TUNEL) assaying was implemented with manufacturer's protocol (Sigma-Aldrich). Slides were examined using a Leica DM600 light microscope to detect apoptotic or necrotic cells. Digital images were captured using a BF450C camera for H&E and a FF363x camera for TUNEL.

6 Statistical analysis

Student's *t* test (two-tailed) was used to calculate statistical significance. Data were considered significantly different when $p < 0.05$.

Data availability statement

All data supporting the findings of this study are available within the paper and its Supplementary Information. Source data are provided with this paper. Any further related information can be provided by the corresponding author upon reasonable request.

References

48. Sauvage, F. *et al.* Photoablation of Human Vitreous Opacities by Light-Induced Vapor Nanobubbles. *ACS Nano* **13**, 8401–8416 (2019).

49. ANSI Z136.1 (2014) - Safe Use of Lasers (Electronic Version). *The Laser Institute* https://www.lia.org/store/product/ansi-z1361-2014-safe-use-lasers-electronic-version (2015).

Supplementary Information

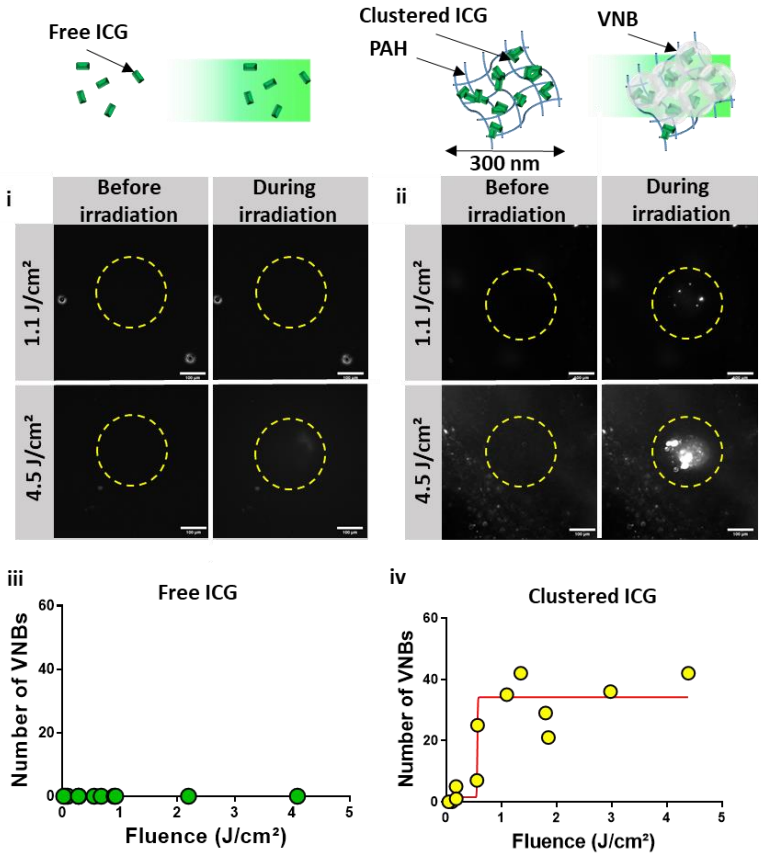

Figure S1. Representative dark field images (n=3 independent experiments) of (i) ICG solutions (0.5 mg/mL) and (ii) dispersions of PAH-ICG nanoparticles (0.5 mg ICG/mL) before and during irradiation with a single laser pulse at 1.1 and 4.5 J/cm² (<7ns; 561 nm); the scale bar is 100 µm. PAH stands for poly(allylamine). (iii, iv) Number of VNBs observed in the irradiated region upon applying a single laser pulse of varying laser fluence.

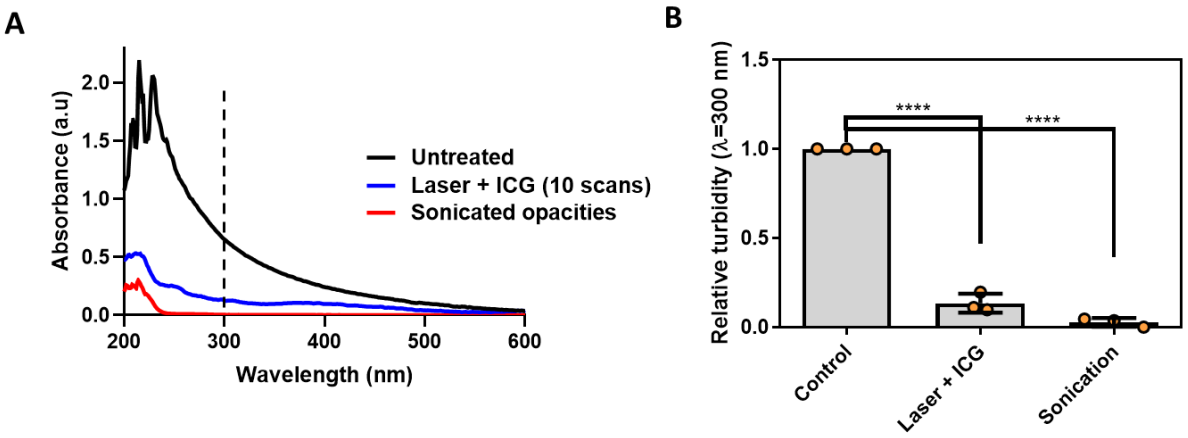

769

770 **Figure S2**. (A) Representative absorption spectra of suspensions of collagen opacities (type I
771 collagen fibers), respectively before and after treatment with ICG (0.5 mg/ml) and irradiated
772 with laser pulses (10 pulses; 561 nm; <7ns; 4.5 J/cm²). Sonicated suspensions of collagen
773 opacities served as positive control (a tip sonicator was used; 30s x 2; 10% amplitude). In these
774 experiments, 50 µL of a suspension of collagen opacities (n=3) in water was completely
775 scanned 10 times with the laser at a fluence at which we could not observe the opacities anymore
776 through dark field imaging (4.5 J/cm²) – subsequently, the samples was removed and absorption
777 spectra were measured with the Nanodrop. (B) Changes in absorption (at 300 nm). n=3
778 independent experiments, data are presented as mean ± s.d, student's *t* test (two-tailed), ****,
779 P<0.0001.

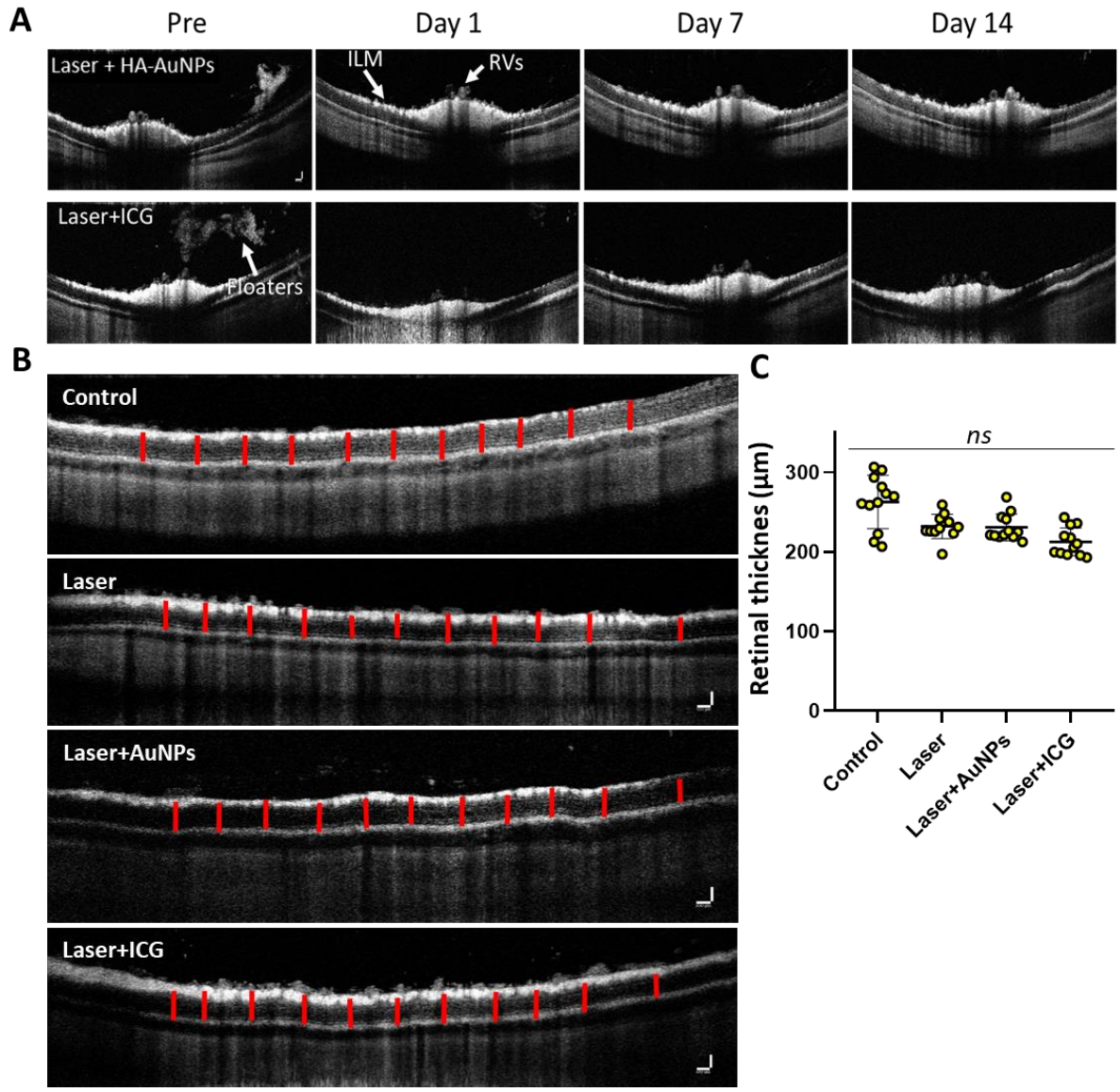

Figure S3. (A) Cross-sectional B-scan OCT images of the retina of rabbits intravitreally injected with HA-AuNPs (top row) and ICG (bottom tow), respectively before and at different time points (1, 7 and 14 days) after laser treatment (1.9 J/cm²; 532 nm (AuNPs), 800 nm (ICG)). All the retinal structures such as retinal vessels (RVs) and internal limiting membrane (ILM) did not show any disorganization or damages. (C) The thickness of the retina of the treated eyes was not significantly different from that of (control) untreated eyes (n= 12 measurements (as indicated by red bars in B) done on a representative OCT image of the retina, data are presented as mean ± s.d, student's *t* test (two-tailed), ns, not significant).

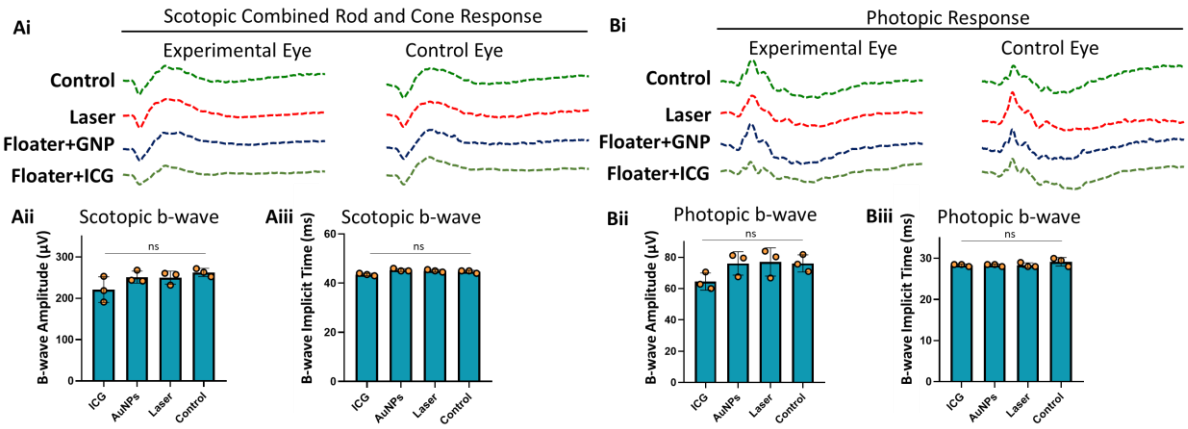

790

791 **Figure S4.** Representative electroretinography waveforms of control and experimental eyes
792 were shown in the left panel at each time point. (Ai) and (Bi) Comparison combined rod-cone
793 ERG waveforms and light-adapted ERG obtained from different treatment groups (control,
794 laser, laser+ICG, and laser+HA-AuNPs). (Aii) and (Aiii) b-wave average amplitude and
795 implicit time of scotopic combined rod-cone response. (Bii) and (Biii) Graph of photopic b-
796 wave average amplitude and implicit time, respectively. n=3 rabbits, data are presented as mean
797 ± s.d, student's *t* test (two-tailed), ns, not significant.

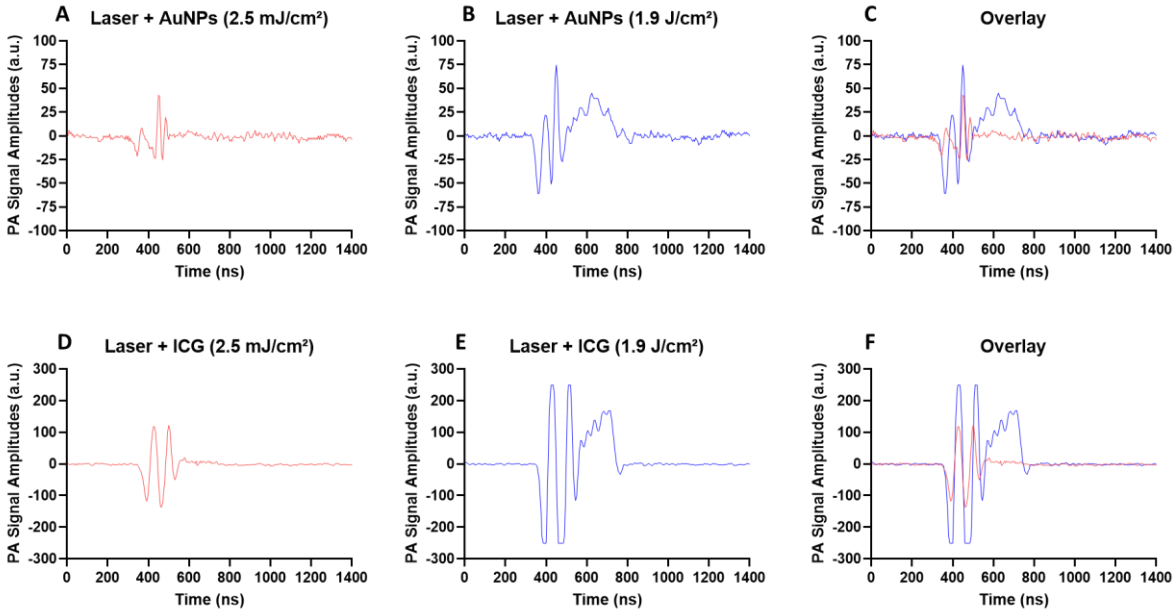

798

799 **Figure S5**. Photoacoustic signals, as monitored with the needle hydrophone, in the vitreous of
800 rabbits. PA signals were recorded at the location of the opacity in the vitreous of rabbits
801 intravitreally injected with AuNPs (top row) or ICG (bottom row). A and D show representative
802 PA-signals as acquired when the laser operates in the imaging mode (2.5 mJ/cm^2; i.e. absence
803 of nanobubbles). B and E show representative PA-signals as acquired during laser treatment

(1.9 J/cm^2) of the opacities (i.e. presence of nanobubbles). C is the overlay of A and B while F is the overlay of D and E. The presented data is representative of experiments performed on n=3 rabbits.

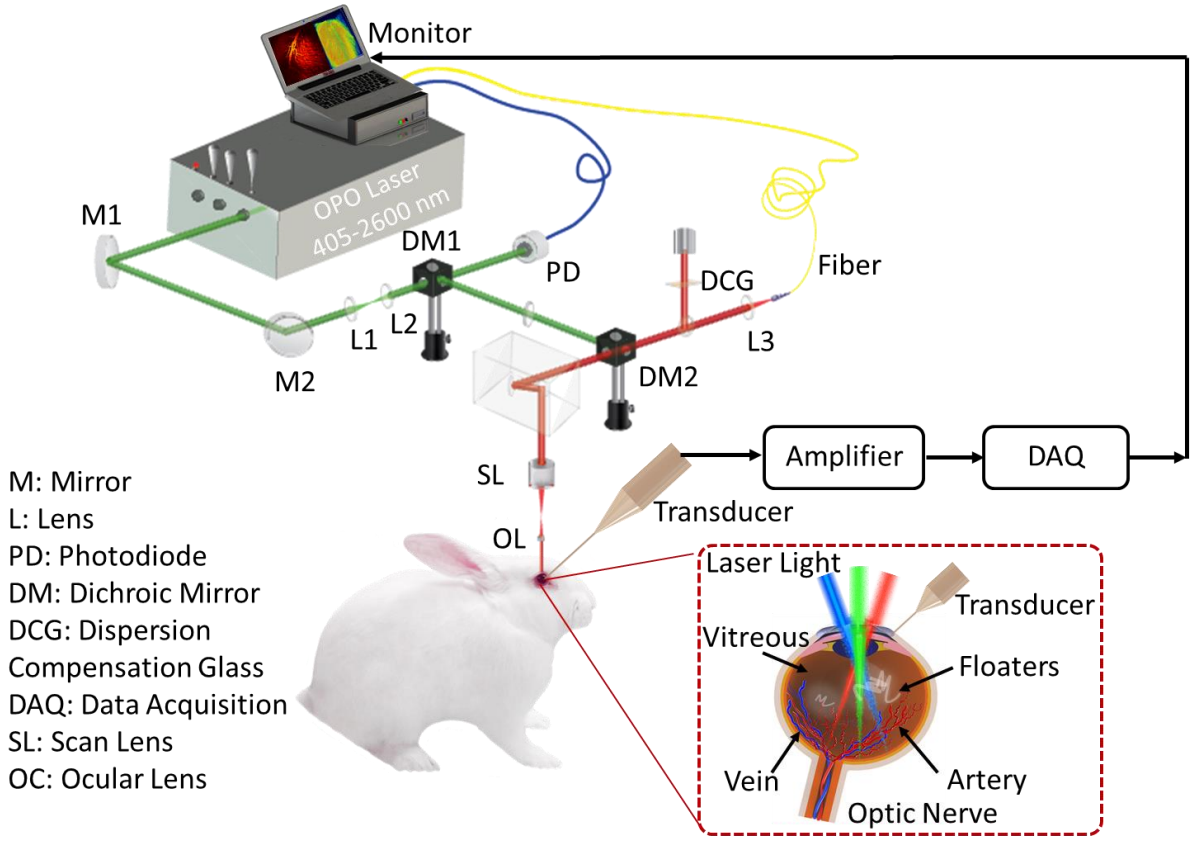

Figure S6. Experimental setup as used for imaging and *in vivo* nanobubble ablation of opacities in the vitreous of rabbits.